ADVANCED FUNCTIONAL MATERIALS
www.afm-journal.de

Molecular or Nanoscale Structures? The Deciding Factor of Surface Properties on Functionalized Poly(3,4-ethylenedioxythiophene) Nanorod Arrays

Hsing-An Lin, Shyh-Chyang Luo, Bo Zhu,* Chi Chen, Yoshiro Yamashita,* and Hsiao-hua Yu**

Nanostructures of poly(3,4-ethylenedioxythiophene) (PEDOT) are assembled by using an anodic aluminum oxide template directly fabricated on gold-coated silicon wafers. Inside these templates, PEDOT and hydroxy functionalized PEDOT form tubes. On the other hand, alkyl- and perfluoro-functionalized PEDOTs assembled as nanorods. This approach allows a platform to understand the molecular and nanostructural effect on the surface wettability of these materials. In the water/air interface, the contact angle of water droplet (CA_{water}) for the smooth alkyl-functionalized PEDOT films increases when alkyl chain gets longer. In contrast, the contact angle reachs saturation at 130° with alkyl chain longer than ethyl in assembled nanorod arrays. It remains the same even in the case of perfluoro-functionalized PEDOT. Moreover, ethyl-functionalized PEDOT (PEDOT-C2) nanorods displays superoleophilicity and the oil deoplet cannot stay on the film in water. Based on the wettability studies, it is concluded that the nanostructures contribute predominantly for the surface wettability of these nanomaterials when the length of alkyl chain crosses certain threshold.

1. Introduction

Nano-assemblies of electrical conducting polymers have recently been recognized as a very critical aspect for functional organic devices.[1–4] They not only provide materials with high surface-to-volume ratio but also allow functional anions or electrons to rapidly diffuse in and out of the materials. For example, nano-sized phase organization of poly(3-hexylthiophene) has been demonstrated as the main deciding factor for enhancing performance of polymer-based bulk heterojucntion solar cells,[5] and a majority of research efforts focus on creation of adequate nanostructure to enhance the energy conversion efficiency. On the other hand, nanostructured conducting polymers have been demonstrated recently useful for bioengineering applications.[6–11] It is not only due to their stability in aqueous solution and biocompatibility,[12,13] but also due to their superior physical and chemical properties enhanced with nanostructural ordering. In a recent report, the suitable nanostructure of carboxylic acid functionalized poly(3,4-ethylenedioxythiophene) (PEDOT)[14] enabled higher capturing efficiency of circulating tumor cells, which is critical for cancer diagnostic and management.

In both organic electronics[15–17] and bioengineering applications,[18–20] surface wettability of the polymer materials exhibits as an important physical characteristic, and it is commonly decided by both chemical composition and surface morphology.[21–23] We previously reported that the increase of roughness of perfluoroalkyl group functionalized PEDOT by different electrical pulse during polymerization results in the contact angle increase of water droplet from 110° to 170°.[24] Guittard and coworkers have reported on the control of surface wettability of perfluoro polymers by a variety of molecular designs.[25,26] In these reports, molecular designs lead to different nanostructures, eventually resulting in the difference of surface hydrophobicity and superhydrophobicity. More recently, both Guittard's and our group demonstrated that similar nanostructures with different conjugated polymer molecular entities amplify the difference in contact angles of liquid droplet.[27,28] Therefore, the molecular structures also contribute to the variation of surface wettability.

In all the cases mentioned above, nanostructures are formed using a template-free assembling approach. Therefore, the molecular architecture determines the major and minor dimensions of the nanostructures. The features observed by electron microscope image may look similar but

H.-A. Lin, Dr. S.-C. Luo, Dr. B. Zhu,
Dr. H.-H. Yu
Yu Initiative Research Unit
RIKEN Advanced Science Institute
2-1 Hirosawa, Wako, Saitama 351-0198, Japan
E-mail: scluo@riken.jp; bzhu@riken.jp; bruceyu@riken.jp
H.-A. Lin, Prof. Y. Yamashita
Department of Electronic Chemistry
Interdisciplinary Graduate School of Science and Engineering
Tokyo Institute of Technology
Nagatsuta, Midori-ku, Yokohama 226-8502, Japan
E-mail: yoshiro@echem.titech.ac.jp
Dr. C. Chen
Nanophotonics Laboratory
RIKEN Advanced Science Institute
2-1 Hirosawa, Wako, Saitama 351-0198, Japan

DOI: 10.1002/adfm.201203006

not identical. As a result, it would be very difficult to rationalize if the property improvement is directly contributed from molecular design or *via* nanostructural effect originated from molecular architect. This differentiation, in our opinion, is critical for further development of materials to provide practical functions. Herein, we would like to demonstrate a platform with electrodepoisted nanorod arrays of PEDOTs containing various side-chains and rationalize in more detail how the chemical composition and surface morphology contribute to the surface properties of these PEDOT nanomaterials.

2. Results and Discussion

There are various approaches to obtain conducting polymer nanorods by hard template,[17,29] soft template,[20] and template-free approaches.[30,31] In order to obtain conducting polymer nanorod arrays with fixed size and density, the most accessible route is to utilize electropolymerization in porous membranes of polycarbonate or anodized aluminum oxide (AAO). These membranes are either commercially available or easily prepared by anodization of aluminum foil.[32] However, transferring the nanorods assembled in the pores onto substrates or devices has proved challenging. This approach is also not adequate to fabricate large area of nanostructured conducting polymers without defects or on patterned devices. Therefore, we would like to adopt herein an approach by directly fabricating AAO membranes on conductive substrates in order to avoid the challenge mentioned above.[33,34] The fabrication and assembly approach we utilized is summarized in **Scheme 1**. It includes 3 main steps: (1) fabrication of porous AAO membrane on conductive substrates, (2) electrodeposition and assembly of functionalized PEDOT materials in the porous AAO template, and (3) dissolution of the AAO template to yield Functionalized PEDOT nanorod arrays.

2.1. Direct Fabrication of Porous Anodic Aluminum Oxide (AAO) on Conducting Substrates

In the majority research effort utilizing porous AAO templates to fabricate conducting polymer nanorods, free standing porous AAO membranes were chosen because they can easily be obtained commercially or anodized from aluminum foil. Unfortunately, it was also very difficult to transfer the nanorods onto substrates to form large area of homogenous and well-organized nanorod arrays. Therefore, we would like to directly fabricate the porous AAO template onto the device through metal deposition and anodization.

An aluminum-covered gold substrate was prepared by depositing 1.2 μm of aluminum layer on a gold substrate using the electron beam physical vapor deposition (EBPVD). The gold substrate was prepared by sequentially depositing 10 nm of titanium (Ti) and 50 nm of gold onto a silicon wafer. A two-step anodization process was adopted to construct the AAO template with ordered-cylindrical pore structures. The inter-pore's distance and pore's diameter of AAO template could be tuned by changing anodization conditions and pore widening treatments.[35,36] After many trials, an anodization process with optimized time and temperature control was finally achieved to fabricate a large area (1.2 cm^2) of AAO template with well defined and organized pores. First, the aluminum-covered substrates were anodized in 0.3 M oxalic acid solution at 15°C by applying a voltage at 40 V for 2.5 min. A thin alumina layer with irregular pores was generated. The initial pore structures are not well-defined as the pore formation started from pits at the aluminum surface. Then the samples were dipped into the phosphoric acid (6%) and chromic acid (1.6%) to dissolve the irregular aluminum oxide layer. A barrier layer with a uniform texture (see Supporting Information Figure S1a) was exposed by removal of the irregular alumina layer. The well defined texture on the barrier layer ensured the formation of uniform and regular pores on alumina substrate during the second anodization step. Second anodization was performed under identical condition to the first anodization, and an AAO template with regular cylindrical pores the template was obtained on gold substrates whereas a barrier layer was presented between the membrane and the conducting substrate. Eventually, the conducting substrates with the AAO template were immersed into 6 wt% phosphoric acid to dissolve the barrier layer and widen the pore diameter to desired size.

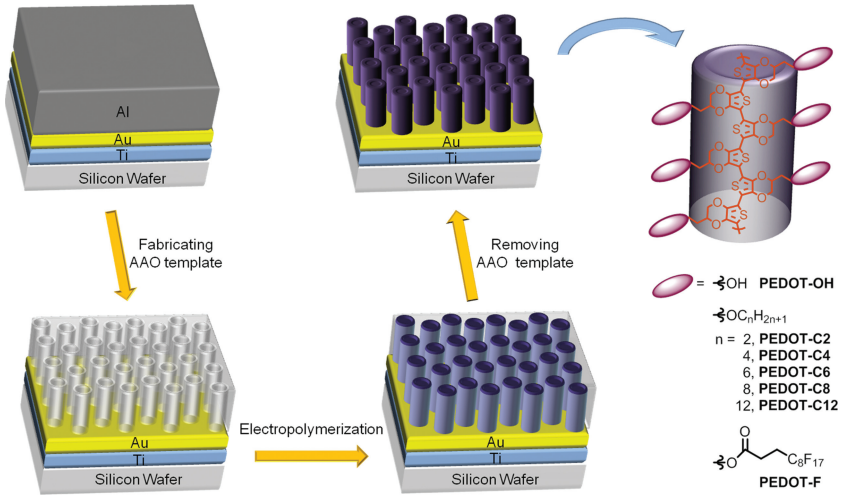

Scheme 1. Schematic illustration of the fabrication of alkyl- and perfluoro-functionalized PEDOTs nanorod arrays.

As shown in **Figure 1**, these fabricated AAO templates presented ordered and uniform pore structures. The thickness and pore size of the AAO templates were 0.9 μm and 60 nm, respectively. However, the AAO templates did not exhibit hexagonal closed packed pores as AAO membranes from free-standing aluminum foils. In addition, we also tried to fabricate the AAO template conductive indium-tin-oxide (ITO) coated glass with a titanium adhesive layer. Although similar porous AAO membranes were obtained (Supporting Information Figure S1b,c),

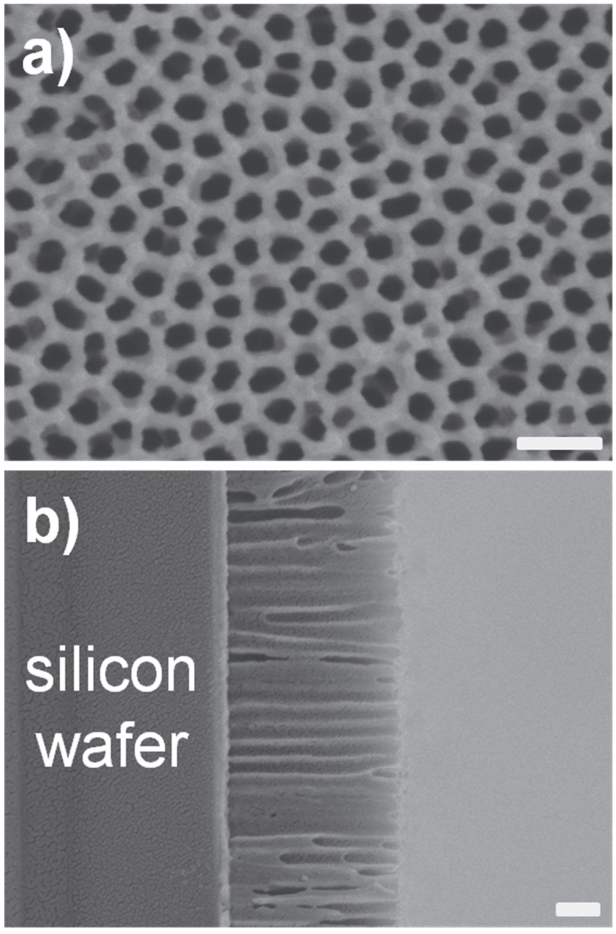

Figure 1. SEM images of a) top view and b) side view of anodic aluminum oxide (AAO) template directly fabricated on gold-coated silicon wafer. The scale bar represents 200 nm.

electropolymerization of PEDOTs could not perform inside these pores. This was most likely due to the formation of insulating titanium dioxide on the bottom of AAO pores during the anodization process (Supporting Information Figure S1d) from titanium oxidation.[37,38] Therefore, electropolymerization inside the pores was hindered. In order to increase the conductivity of the adhesion layer, we tried to deposit a thin layer of gold between titanium adhesion layer and the thicker aluminum layer. Unfortunately, this layer of gold resulted in the detachment of AAO templates when the second anodization was performed. At the end, we were unable to obtain the similar PEDOT nanorod arrays on ITO-coated glasses.

2.2. Electropolymerization and Assembly of PEDOTs in the AAO Template

AAO templates have been demonstrated successfully to be utilized for electro-deposition of one-dimensional conducting polymer nanostructures after a conductive metal layer was coated on the membrane. However, it is also challenging to tansfer the nanostructures onto substrates to yield nanostructure arrays. In our platform, the AAO layer which was fabricated directly on the conducting substrate could serve as an integrated substrate and template. Therefore, conduting polymer nano arrays within large area of conductive substrates were formed without the necessity of structure transfer. Previously, unfunctionalized PEDOT nanowires and nanotubes were successfully deposited and assembled in gold- or silver-coated alumina membranes by carefullly controlling the monomer concentration and applied voltage.[29] Typically, this procedure was achieved by applying constant voltage for a longer period of time (100 s) at low monomer concentration (0.01 M) in solution. However, similar results with the formation of uniform nanotubes or nanorods in our platform using identical experimental conditions did not occur. This could be due to the smaller pore size (60 nm, comparing to 200 nm in commerical AAO templates) of the AAO membrane we used in order to obtain smaller size features. The pore size confined spatially not only the growth of conducting polymer but also the diffusion of monomer. As a result, we observed a high concentration of EDOT monomer solution (0.1 M) provided better experimental results for the electropolymerization in our AAO template. The initial attempt to conduct electropolymerization by applying a constant voltage of 1.6 V for 7 s in 0.1 M EDOT monomer solution resulted in the formation of tubular assemblies inside the pores of AAO (as shown in Supporting Information Figure S2a). However, these nanotubes presented uneven surface morphology and the top of the nanotubes collapsed together due to the weaker mechanical properties of the tubes. We suspected that the high applied potential and monomer concentration acceleated the rate of electropolymerization, which resulted in less control over assmbly and size distribution due to the non-synchronized nucleation process.

One approach to control the kinetic parameters of electropolymerization is to provide a rest period after triggering the electropolymerization with a very short pulse of applied oxidation potential.[39,40] After several trials, we found the rest period with the applying voltage at 0 V allowed uniform growth of conducting polymers among all pores. As shown in Supporting Information Figure S2b, the initial attempt to utilize pulsed oxidation potential (1.6 V for 0.1 s followed by 0 V for 1 s for 30 cycles) resulted in much more uniform growth of PEDOT nanotubes inside the pores of AAO membrane. On the other hand, the high concentration of EDOT monomers and high applied voltage were still not ideal. Eventually, we obtained an optimized condition with a reduced monomer concentration (0.01 M), lower oxidation potential and longer relaxed time (1.2 V for 0.1 s followed by 0 V for 2 s). Unfunctionalized PEDOT nanotube arrays were able to be fabricated as shown in **Figure 2**a.

2.3. Formation of Functinalized PEDOT Nano rod Arrays

After successfully electrodeposite unfunctionalized PEDOT nanotubes in the pores of AAO membranes, the AAO membranes were dissolved in 1 M NaOH solution after immersing the device for 30 min. Transmission microscope (TEM) images confirmed that the nanostructures formed were nanotubes (Figure 2d). These approach was then expanded to EDOT monomers bearing various functional groups. As shown in Figure 2, we noticed

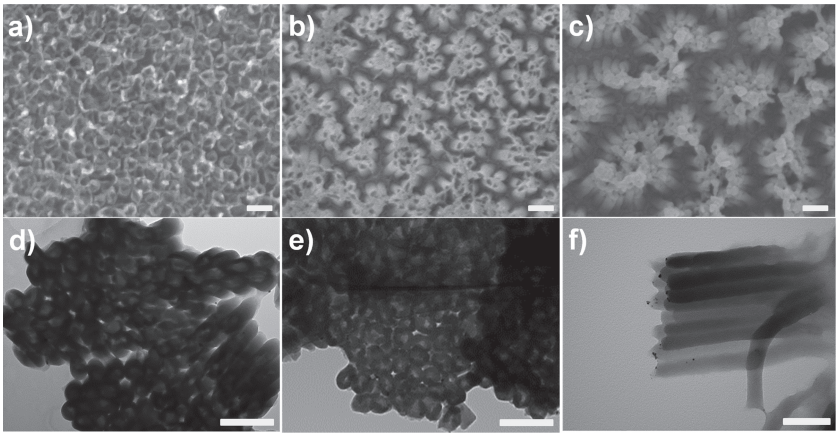

Figure 2. SEM images of a) PEDOT, b) PEDOT-OH, c) PEDOT-C8 and TEM images of d) PEDOT, e) PEDOT-OH, f) PEDOT-C8. These nanostructures are directly assembled inside AAO templates and the scale bar represents 200 nm.

significant difference in the electrodeposition and assembly inside the pores of AAO template when different monomers were used. In the case of PEDOT and PEDOT-OH (Figure 2b,e), nanotubular structures were formed. However, when more hydrophobic monomer, EDOT-C8, was electrodeposited into the pores, we observed the formation of nanorods instead of nanotubes. The reasons for the formation of different nanostructures were not well understood. Our findings were also different from studies with free-standing aluminum membranes. The AAO template we fabricated directly onto devices was thinner than the commerically available AAO membranes. Therefore, the nanostructures were influenced by the surface interactions and the deposited materials more. In principle, the surfaces of AAO membranes are more hydrophilic because of the polar -OH groups presented. As a result, more hydrophilic PEDOT and PEDOT-OH would prefer to adhere to the surfaces on the bottom and wall of AAO membranes and assemble as tubular structure without filling the pores. In contrast, more hydrophobic PEDOT-C8 would love to fill in the pores evenly because it did not favor interactions to the template's surface. As a result, nanorods were formed.

In order to further evaluate the electropolymerization, we analyzed the chronoamperometric response of the electropolymerizaton with the application of pulsed potential. As shown in Supporting Information Figure S3b,c, more EDOTs were electropolymerized in solution with higher EDOT concentration, indicated by the higher current recorded when the potential was applied. This supported our earlier observation that it was critical to conduct electropolymerization with higher monomer concentration because the pore of AAO membrane was small and limited the diffusion of monomers. The comparion between electropolymerization of EDOT (lower current recorded in Supporting Information Figure S3b) and EDOT-C12 (higher current recorded in Supporting Information Figure S3d) also indicated that more polymers were deposited in the AAO pores. The results confirmed the difference of the formation of nanotubes and nanorods since more materials are required to fill in the pores in order to form nanorods.

Previously, there were several reports discussing on the nanostructured conducting polymers and their effects on the surface properties, particularly at the air-water interface. However, it remains a great challenging to understnd the individual effects of molecular structures and nanostructures on the property. In these reports, molecular designs lead to different nanostructures, eventually resulting in the difference of surface hydrophobicity and superhydrophobicity. With the functionalized PEDOT nanorod arrays, we had an ideal platform to study this question because we could fabricate identical nanostructures with different molecular structures. We directly fabricated nanorod arrays of PEDOT-C2, -C4, -C6, -C8, -C12 and –F using identical AAO porous templates. The SEM and TEM images of the nanorod arrays are shown in **Figure 3** and **Figure 4**. The SEM images indicated that most of nanorods were aggregated at the top end of the rods at dried state after removing the AAO template. However, they might be isolated while immersing in the aqueous solution. The TEM images shown in Figure 4 provided strong evidences that no tubular section occurred along the rods. The average length and diameter of nanorods were 500 and 50 nm, respectively. The aggregation of the PEDOT nanorods was most likely due to their weaker mechanical properties. As a result,

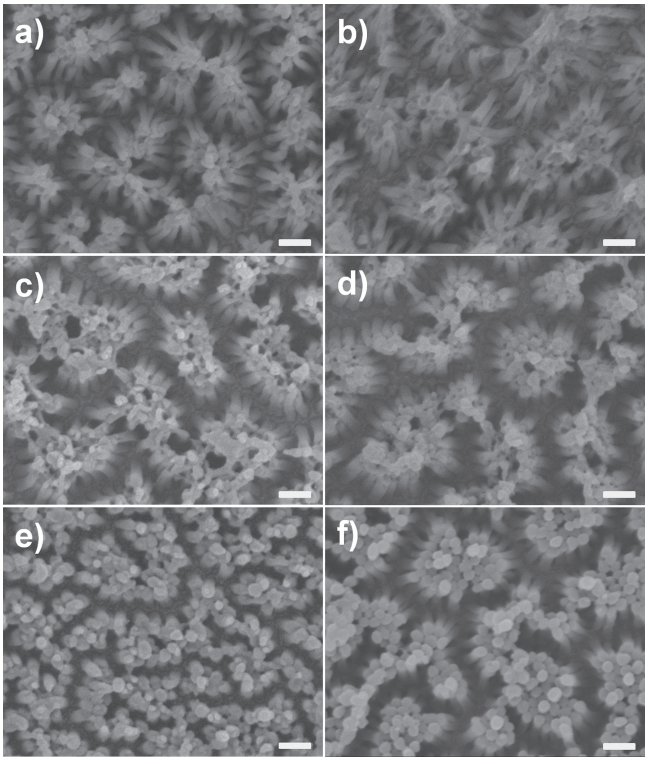

Figure 3. SEM images of nanorod arrays assembled from alkyl- and perfluoro-functionalized PEDOT: a) PEDOT-C2, b) PEDOT-C4, c) PEDOT-C6, d) PEDOT-C8, e) PEDOT-C12 and f) PEDOT-F. The scale bar represents 200 nm.

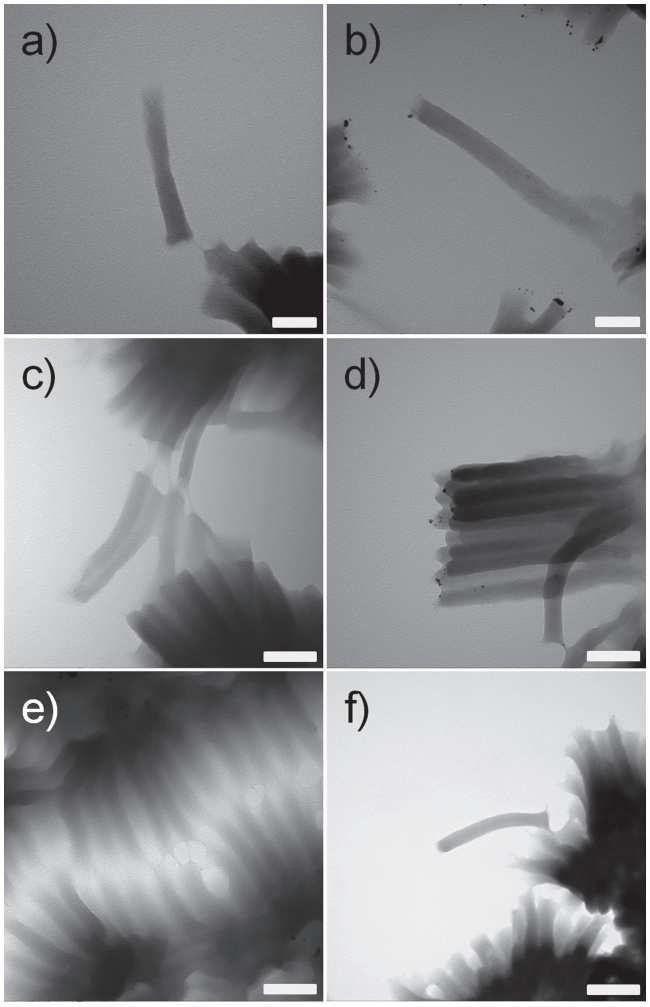

Figure 4. TEM images of nanorod arrays assembled from alkyl- and perfluoro-functionalized PEDOT: a) PEDOT-C2, b) PEDOT-C4, c) PEDOT-C6, d) PEDOT-C8, e) PEDOT-C12 and f) PEDOT-F. The scale bar represents 100 nm in (a) and (b) and 200 nm in (c) - (f).

the structure could not hold straight at dried states when the nanorods exhibited with high aspect ratio. As control experiments, we also fabricated uniform thin films of all functionalized PEDOTs. Their SEM images summaized in **Figure 5** confirmed that the surface was smooth. The roughness of the films was measured by atomic force microscope (Supporting Information Figure S4) and the root-mean-square roughness of the films was all below 5 nm.

2.4. Nanoscale and Molecular Structure Effects on Surface Properties of Conducting Polymers

The wettability of functionalized PEDOT films and nanorod arrays were evaluated by measuring the static contact angles of water droplets in air and hexadecane droplets in water as shown in **Figure 6**, and all the results were summarized in **Table 1**. Based on the definition,[41] when the surface's contact angle of

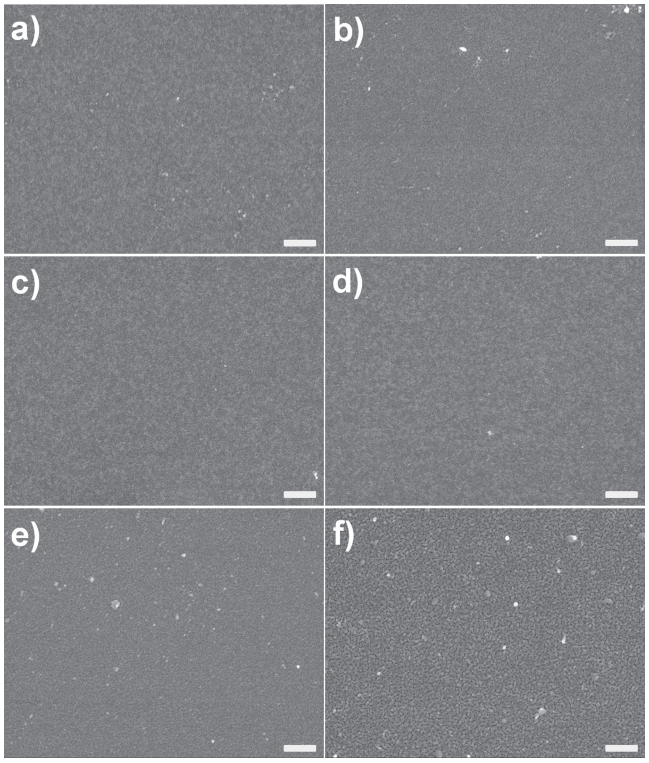

Figure 5. SEM images of films from alkyl- and perfluoro-functionalized PEDOT: a) PEDOT-C2, b) PEDOT-C4, c) PEDOT-C6, d) PEDOT-C8, e) PEDOT-C12, and f) PEDOT-F. The scale bar represents 400 nm.

water (CA_{water}) is below 90°, the surface is defined hydrophilic surface, whereas the surface is defined hydrophobic surface when CA_{water} is above 90°. The CA_{water} of **PEDOT-C2, -C4** and **-C6** films were below 90°, which indicates more hydrophilic surfaces. On the other hands, the CA_{water} of **PEDOT-C8, -C12** and **-F** films were 94°, 97.5°, and 110.5°, respectively, which indicate more hydrophobic surfaces. The CA_{water} of **PEDOT-F**

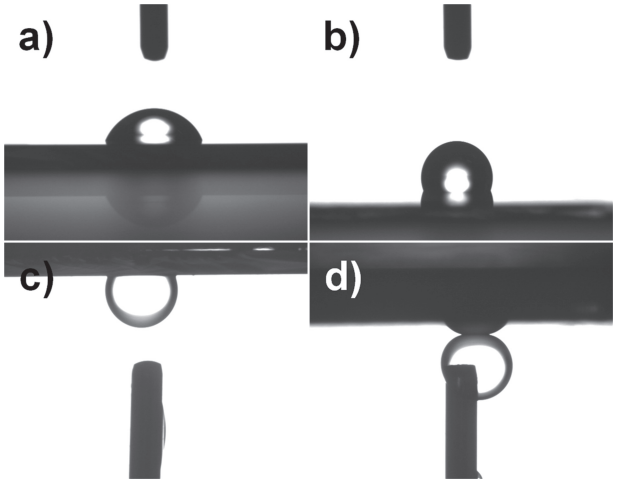

Figure 6. Images of water droplets on PEDOT-C2 surfaces: a) film and b) nanorod array. Images of oil droplets in water on PEDOT-C2 surfaces: c) film and d) nanorod array.

Table 1. Contact angles of water and oil (hexadecane) droplets on films and nanorod arrays from alkyl- and perfluoro-functionalized PEDOTs.

polymers	CA_{water} [°] on film	CA_{water} [°] on nanorod array	$CA_{oil\ in\ water}$ [°] on film[a)]	$CA_{oil\ in\ water}$ [°] on nanorod array
PEDOT-C2	65.6 ± 1.6	109.2 ± 1.2	109.0 ± 1.7	[b)]
PEDOT-C4	83.8 ± 0.8	128.7 ± 0.9	100.4 ± 1.8	136.6 ± 0.3
PEDOT-C6	84.5 ± 1.2	130.8 ± 1.8	99.3 ± 0.1	119.8 ± 1.2
PEDOT-C8	94.0 ± 0.7	132.5 ± 0.9	80.6 ± 0.8	84.8 ± 1.0
PEDOT-C12	97.5 ± 0.8	129.7 ± 0.4	80.2 ± 2.0	84.3 ± 1.4
PEDOT-F	110.5 ± 0.5	130.6 ± 1.3	80.5 ± 1.7	91.8 ± 0.7

[a)]Oil is hexadecane; [b)]Oil droplets cannot be placed on the surface.

film was higher than alkyl functionalized PEDOT films because perfluoro chain provided lower surface energy than alkyl chain.[42] Although the morphology and the roughness of alkyl functionalized PEDOT films were quite similar, the CA_{water} of the films increased when the alkyl chain length increased. This indicates the chemical structures change surfaces properties and the increase of alkyl chain length makes surfaces more hydrophobic. Previous studies,[43] also show that the increase of alkyl chain length can induce the formation of different micro/nanostructures and achieve superhydrophobic surfaces. Different from their research interests, here we would like to understand how these side chains solely affect on the surface properties when their nanostructures are similar. The CA_{water} of **PEDOT-C2**, **-C4**, **-C6**, **-C8** and **-C12** with similar nanorod structures were 109.2°, 128.7°, 130.8°, 132.5°, and 129.7°, respectively. Generally, the CA_{water} of functionalized PEDOT nanorods were higher than PEDOT films due to nano-effect enhancement.[26] When alkyl chain length was longer than ethyl unit, the CA_{water} of alkyl functionalized PEDOTs with nanorod structures were around 130°. The different chain lengths didn't dramatically influence the contact angle when the surfaces present similar nanostructures. The CA_{water} of **PEDOT-F** was also around 130° even though **PEDOT-F** contained perfluoro side-chain which is usually used for achieving superhydrophobic surface. Although the wettability of the surface is usually governed by both the chemical composition and the morphology of the surface, our results showed that the CA_{water} of PEDOT nanorod arrays didn't increase as obviously as CA_{water} of PEDOT films when the side chain length is longer than **C4**. The underwater wettability plays an important role in many applications, such as microfluidic technology,[44] bioadhesion,[45] and marine antifouling materials.[46] In recent reports, nanostructured polypyrrole and polyaniline were investigated their underwater wettability for demonstrating reversible switch between superoleophobicity and superoleophilicity,[47] and oil droplet transport.[48] In this report, hexadecane was used as oil droplets in the investigation of underwater wettability. The underwater contact angle of oil ($CA_{oil\ in\ water}$) of **PEDOT-C2**, **-C4**, **-C6**, **-C8**, **-C12** and **-F** films were 109.0°, 100.4°, 99.3°, 80.6°, 80.2° and 80.5°, respectively. The contact angle decreased when the chain length increased until to **C8**. The surfaces of PEDOT with octyl, dodecyl and perfluoro chains all exhibited similar $CA_{oil\ in\ water}$ around 80°. The nano-effect was also observed on the contact angle in oil in water system as shown in Figure 5c,d. The $CA_{oil\ in\ water}$ of **PEDOT-C4**, **-C6**, **-C8**, **-C12** and **-F** with nanorod structures were 136.6°, 119.8°, 84.8°, 84.3° and 91.8°, respectively. Surprisingly, the oil droplets could not stay onto the surface of **PEDOT-C2** with nanorod structure in water as shown in Figure 5d. It may be because that the ethyl chain in PEDOT was too short to cover the hydrophilic PEDOT backbone. The hydrophilic backbone did not allow oil droplet to attach on the surface, which indicates a superoleophobic surface by nanostructured **PEDOT-C2** surfaces. One more thing to be pointed out here is, **PEDOT-C8** and **PEDOT-C12** showed similar both CA_{water} and $CA_{oil\ in\ water}$ when the surfaces with similar nanorod structure. This indicates that chain length effect on the nanostructures is not as dominates as on smooth films when the PEDOT with octyl and longer alkyl chains. In other words, the structure effect plays a more important role when the alkyl chain is longer.

3. Conclusions

We have develped herein a hard-template based approch to modify conducting substrates with well defined nanorod arrays of functionalized PEDOTs. Anodic aluminum oxide (AAO) templates are fabricated directly onto the conducting substrate and functionalized EDOT monomers are assembled inside the pores of these AAO templates by applying pulsed voltage to initiate electropolymerization and deposition. It is noticed that hydrophilic monomers (unfunctionalized EDOT and EDOT-OH) formed tubes inside the pores. On the other hand, alkyl and perfluoro-functionalized PEDOTs are assembled as rods with almost identical nanostructures. These ordered nanorod arrays allow us to diffrentiate the contribution of molecular architecture and micro/nanoscale structures on the surface properties of our materials. In the water/air interface, the contact angle of water droplet (CA_{water}) for the smooth alkyl functionalized PEDOT films increases when alkyl chain gets longer. At the same time, the contact angle reachs saturation at 130° with alkyl chain longer than C2 in assembled nanorod arrays. Moreover, the perfluoro-functionalized PEDOT with identical nanostructures also shows contact angle around 130°. In the oil/water interface, the contact angle of oil droplet ($CA_{oil\ in\ water}$) on films or nanorod arrays of alkyl- and perfluoro-functionalized PEDOTs decreases with longer alkyl chains. The contact angle only reaches saturation in the nanorod arrays when the chain is longer than C8. In a word, our results show that the

nanostructural effect dominates the surface wettability of the PEDOT nanorod arrays when the length of alkyl chain crosses certain threshold. It is also noticeable that **PEDOT-C2** nanorod array displays superoleophobicity in water. This material shows potential applied as underwater self-cleaning material.

4. Experimental Section

Monomer Synthesis: All chemicals were purchased from Sigma-Aldrich. The EDOT with alkyl[49,50] and perfluoro[51] substituent were synthesized by following previous reports. As described below is the synthesis procedure of the monomers.

EDOT-C2: A mixture of NaH (3.48 g, 145 mmol) and 18-crown-6 ether (0.767 mg, 2.9 mmol) dissolved in anhydrous THF (70 mL) was stirred under nitrogen at 0 °C. 2,3-Dihydrothieno[3,4-b][1,4]dioxin-2-yl)methanol (EDOT-OH) (5 g, 29 mmol) in 30 mL of anhydrous THF was added. The mixture was stirred at room temperature for 1 h and then cooled down to 0 °C. Bromoethane (3.792 g, 34.8 mmol) was added droplet within 10 min. After stirring at room temperature overnight, the mixture was diluted with 200 mL NH_4Cl aqueous solution. The mixture was extracted with dichloromethane (200 mL) three times. The combined organic phases were washed with water, dried over $MgSO_4$, and evaporated in vacuo. The crude product was purified by flash chromatography (ethyl acetate/hexane = 1/5) to yield a colorless oil (5.00 g, 86%). ^{1}H NMR (500 MHz, $CDCl_3$, δ): 6.34-6.32 (m, 2H), 4.32-4.28 (m, 1H), 4.25 (dd, J = 11.5, 2.0 Hz, 1H), 4.06 (dd, J = 11.5, 7.5 Hz, 1H), 3.67 (dd, J = 10.5, 5.5 Hz, 1H), 3.60 (dd, J = 10.0, 6.0 Hz, 1H), 3.56 (t, J = 7.0 Hz, 2H), 1.22 (t, J = 7.0 Hz, 3H). ^{13}C NMR (500 MHz, $CDCl_3$, δ): 141.6, 141.5, 99.7, 99.5, 72.7, 68.9, 67.3, 66.2, 15.1; HRMS (EI) m/z: [M$^+$] calcd for $C_{11}H_{16}O_3S$; 200.0507; found, 200.0507.

Using the same procedure for **EDOT-C2**, the following compounds were prepared: **EDOT-C4**: This yielded a colorless oil (5.28 g, 80%). ^{1}H NMR (500 MHz, $CDCl_3$, δ): 6.33-6.31 (m, 2H), 4.32-4.28 (m, 1H), 4.24 (dd, J = 11.5, 2.0 Hz, 1H), 4.05 (dd, J = 11.5, 7.5 Hz, 1H), 3.68 (dd, J = 10.5, 5.5 Hz, 1H), 3.59 (dd, J = 10.0, 6.0 Hz, 1H), 3.50 (t, J = 7.0 Hz, 2H), 1.60-1.54 (m, 2H), 1.40-1.33 (m, 2H), 0.92 (t, J = 7.0 Hz, 3H). ^{13}C NMR (500 MHz, $CDCl_3$, δ): 141.6, 141.5, 99.7, 99.5, 72.6, 71.8, 69.1, 66.2, 31.6, 19.2, 13.9; HRMS (EI) m/z: [M$^+$] calcd for $C_{11}H_{16}O_3S$, 228.0802; found, 228.0818. **EDOT-C6**: This yielded a colorless oil (6.25 g, 84%). ^{1}H NMR (500 MHz, $CDCl_3$, δ): 6.33-6.31 (m, 2H), 4.32-4.28 (m, 1H), 4.25 (dd, J = 11.5, 2.0 Hz, 1H), 4.05 (dd, J = 11.5, 7.5 Hz, 1H), 3.68 (dd, J = 10.5, 4.5 Hz, 1H), 3.59 (dd, J = 10.0, 6.0 Hz, 1H), 3.49 (t, J = 7.0 Hz, 2H), 1.61-1.53 (m, 2H), 1.36-1.25 (m, 6H), 0.89 (t, J = 7.0 Hz, 3H). ^{13}C NMR (500 MHz, $CDCl_3$, δ): 141.6, 141.5, 99.6, 99.5, 72.6, 72.1, 69.1, 66.3, 31.6, 29.5, 25.7, 22.6, 14.0; HRMS (EI) m/z: [M$^+$] calcd for $C_{13}H_{20}O_3S$, 256.1133; found, 256.1129. **EDOT-C8**: This yielded a colorless oil (7.00 g, 85%). ^{1}H NMR (500 MHz, $CDCl_3$, δ): 6.33-6.31 (m, 2H), 4.32-4.28 (m, 1H), 4.24 (dd, J = 11.5, 2.0 Hz, 1H), 4.05 (dd, J = 11.5, 7.5 Hz, 1H), 3.68 (dd, J = 10.0, 4.5 Hz, 1H), 3.59 (dd, J = 10.5, 6.0 Hz, 1H), 3.49 (t, J = 7.0 Hz, 2H), 1.60-1.55 (m, 2H), 1.35-1.22 (m, 10H), 0.88 (t, J = 7.0 Hz, 3H). ^{13}C NMR (500 MHz, $CDCl_3$, δ): 141.6, 141.5, 99.7, 99.5, 72.6, 72.1, 69.1, 66.3, 31.8, 29.5, 29.4, 29.2, 26.0, 22.6, 14.1; HRMS (EI) m/z: [M$^+$] calcd for $C_{15}H_{24}O_3S$, 284.1446; found, 284.1448. **EDOT-C12**: This yielded a colorless oil (8.19 g, 83%). ^{1}H NMR (500 MHz, $CDCl_3$, δ): 6.33-6.31 (m, 2H), 4.32-4.28 (m, 1H), 4.25 (dd, J = 11.5, 2.0 Hz, 1H), 4.06 (dd, J = 11.5, 7.5 Hz, 1H), 3.68 (dd, J = 10.0, 4.5 Hz, 1H), 3.59 (dd, J = 10.0, 6.0 Hz, 1H), 3.49 (t, J = 7.0 Hz, 2H), 1.60-1.55 (m, 2H), 1.35-1.22 (m, 18H), 0.88 (t, J = 7.0 Hz, 3H). ^{13}C NMR (500 MHz, $CDCl_3$, δ): 141.6, 141.5, 99.7, 99.5, 72.6, 72.1, 69.1, 66.3, 31.9, 29.7, 29.6, 29.6, 29.6, 29.5, 29.4, 29.4, 26.0, 22.7, 14.1; HRMS (EI) m/z: [M$^+$] calcd for $C_{19}H_{32}O_3S$, 340.2072; found, 340.2074.

EDOT-F:4,4,5,5,6,6,7,7,8,8,9,9,10,10,11,11,11-Heptadecafluoroundecanoic acid (571 mg, 1.16 mmol), *N,N′*-dicyclohexylcarbodiimine (239 mg, 1.16 mmol), and 4-dimethylaminopyridine (14 mg, 0.12 mmol) were dissolved in dichloromethane (15 mL), and the reaction mixture was stirred for 1 h under nitrogen. Afterward, EDOT-OH (200 mg, 1.16 mmol) was added. After stirring at room temperature overnight, the mixture was diluted with 1 M HCl aqueous solution (100 mL). The mixture was extracted with dichloromethane (100 mL) three times. The combined organic phases were washed with water, dried over $MgSO_4$, and evaporated in vacuo. The crude product was purified by flash chromatography (ethyl acetate/hexane = 1/4) to yield a colorless oil (389 mg, 52%). ^{1}H NMR (500 MHz, $CDCl_3$, δ): 6.38 (d, J = 3.7, 1H), 6.37 (d, J = 3.7, 1H), 4.59 (m, 2H), 4.48 (m, 1H), 4.25 (dd, J = 11.5, 2.0 Hz, 1H), 4.08 (dd, J = 11.5, 6.5 Hz, 1H), 2.71 (t, J = 7.2, 2 H), 2.51 (tt, 2 H, J = 18.6 Hz, J = 7.2 Hz). ^{13}C NMR (500 MHz, $CDCl_3$, δ): 170.8, 141.1, 140.8, 100.2, 100.1, 71.2, 65.4, 63.0, 26.4, 25,3. ^{19}F NMR (500 MHz, $CDCl_3$, δ): -126.6, -124.0, -123.2, -122.4, -111.3, -81.3; HRMS (EI) m/z: [M$^+$] calcd for $C_{18}H_{11}F_{17}O_4S$, 646.0107; found, 646.0109.

Fabrication of AAO Template: Ultra high purity of Ti (99.99%), Au (99.99%) and Al (99.99%) are purchased from Furuuchi chemical corporation. An aluminum-covered gold substrate was prepared by an electron beam physical vapor deposition system (EBPVD) (base pressure: $\approx 10^{-5}$–10^{-6} Torr). Depositing rate of Ti, Au and Al are 0.2, 2, ≈3–5 Å s^{-1}, respectively. The Al-covered gold substrates carried out the first-step anodization in 0.3 M oxalic acid solution at 40 V and 15 °C for 2.5 min. After the first-step anodization, the alumina film was removed using a solution of 6 wt% phosphoric acid and 1.6 wt% chromic acid at 40 °C for 22 min. The second-step anodization was performed under the same conditions as the first-step anodization for ≈8–10 min. Finally, the sample was dipped into 6 wt% phosphoric acid at 30 °C for 30 min to dissolve the barrier layer and enlarge pore diameter to desired size.

Electropolymerization: Monomer solutions were prepared by dissolving monomers at concentrations of ≈0.01–0.1 M in acetonitrile containing 0.1 M lithium perchlorate as electrolyte. The electropolymerization was performed by using a potentiostat (PGSTAT128N, Autolab) with a Ag/Ag^+ electrode (RE-7, BAS) as the reference electrode, and a Pt mesh as the counter-electrode. Nanostructured PEDOTs were fabricated by electropolymerization using constant voltage method (1.6 V for 7 s) or pulsed voltage method (1.6 V for 0.1 s followed by 0 V for 1 s, 30 cycles; 1.2 V for 0.1 s followed by 0 V for 2 s, 30 cycles).

Removal of AAO Template: After electrodepositing functionalized and unfunctionalized PEDOT nanostructures in the pores of AAO membranes, the AAO membranes were dissolved in 1 M NaOH solution after immersing the device for 30 min.

Surface Characterization: Scanning electron microscopy (SEM) experiments were conducted using a FE-SEM (JSM-6330F, JEOL) to observe the surface morphology of samples. A thin layer Au (<3 nm) was coated on samples ahead of SEM experiments. Transmission electron microscopy (TEM) experiments were done by a JEM-2100 LaB6 transmission electron microscope at an accelerating voltage of 200 kV. Static contact angle of water (1.4 μL) or hexadecane (1.6 μL) droplet was measured by a contact angle measurement system (Drop Master 500, Kyowa, Inc.). The measurement of each sample was repeated for 3 times.

Supporting Information

Supporting Information is available from the Wiley Online Library or from the author.

Acknowledgements

This work was financially supported by RIKEN Advanced Science Institute and Grant-in-Aid for Young Scientist (No. 22681016 and 23710138) from JSPS/MEXT, Japan. B.Z. thanks RIKEN for a Special Postdoctoral Researcher Fellowship.

Received: October 15, 2012
Revised: December 21, 2012
Published online: February 6, 2013

[1] C. Li, H. Bai, G. Shi, *Chem. Soc. Rev.* **2009**, *38*, 2397.
[2] H. D. Tran, D. Li, R. B. Kaner, *Adv. Mater.* **2009**, *21*, 1487.
[3] D. Li, J. Huang, R. B. Kaner, *Acc. Chem. Res.* **2008**, *42*, 135.
[4] N. S. Ramgir, Y. Yang, M. Zacharias, *Small* **2010**, *6*, 1705.
[5] B. C. Thompson, J. M. J. Fréchet, *Angew. Chem. Int. Ed.* **2008**, *47*, 58.
[6] H. Yoon, S. Ko, J. Jang, *J. Phys. Chem. B* **2008**, *112*, 9992.
[7] N. K. Guimard, N. Gomez, C. E. Schmidt, *Prog. Polym. Sci.* **2007**, *32*, 876.
[8] C. M. Hangarter, M. Bangar, A. Mulchandani, N. V. Myung, *J. Mater. Chem.* **2010**, *20*, 3131.
[9] H. Peng, C. Soeller, J. Travas-Sejdic, *Macromolecules* **2007**, *40*, 909.
[10] M. Berggren, A. Richter-Dahlfors, *Adv. Mater.* **2007**, *19*, 3201.
[11] B. Garner, A. Georgevich, A. J. Hodgson, L. Liu, G. G. Wallace, *J. Biomed. Mater. Res.* **1999**, *44*, 121.
[12] M. Asplund, E. Thaning, J. Lundberg, A. C. Sandberg-Nordqvist, B. Kostyszyn, O. Inganäs, H. v. Holst, *Biomed. Mater.* **2009**, *4*, 045009.
[13] M. Asplund, T. Nyberg, O. Inganäs, *Polym. Chem.* **2010**, *1*, 1374.
[14] J. Sekine, S.-C. Luo, S. Wang, B. Zhu, H.-R. Tseng, H.-H. Yu, *Adv. Mater.* **2011**, *23*, 4788.
[15] H. Yan, K. Kurogi, H. Mayama, K. Tsujii, *Angew. Chem. Int. Ed.* **2005**, *44*, 3453.
[16] B. Su, S. Wang, J. Ma, Y. Wu, X. Chen, Y. Song, L. Jiang, *Adv. Mater.* **2012**, *24*, 559.
[17] J. I. Lee, S. H. Cho, S.-M. Park, J. K. Kim, J. K. Kim, J.-W. Yu, Y. C. Kim, T. P. Russell, *Nano Lett.* **2008**, *8*, 2315.
[18] X. Zhang, F. Shi, J. Niu, Y. Jiang, Z. Wang, *J. Mater. Chem.* **2008**, *18*, 621.
[19] M. Qu, G. Zhao, X. Cao, J. Zhang, *Langmuir* **2008**, *24*, 4185.
[20] H. Yoon, M. Chang, J. Jang, *Adv. Funct. Mater.* **2007**, *17*, 431.
[21] F. Xia, L. Jiang, *Adv. Mater.* **2008**, *20*, 2842.
[22] X. J. Feng, L. Jiang, *Adv. Mater.* **2008**, *18*, 3063.
[23] Y. Zhu, J. Zhang, Y. Zheng, Z. Huang, L. Feng, L. Jiang, *Adv. Funct. Mater.* **2006**, *16*, 568.
[24] S.-C. Luo, S. S. Liour, H.-H. Yu, *Chem. Commun.* **2010**. *46*, 4731.
[25] T. Darmanin, E. Taffin de Givenchy, S. Amigoni, F. Guittard, *Langmuir* **2010**, *26*, 17596.
[26] T. Darmanin, F. Guittard, *J. Am. Chem. Soc.* **2009**, *131*, 7928.
[27] S.-C. Luo, J. Sekine, B. Zhu, H. Zhao, A. Nakao, H.-H. Yu, *ACS Nano* **2012**, *6*, 3018.
[28] T. Darmanin, M. Nicolas, F. Guittard, *Langmuir* **2008**, *24*, 9739.
[29] R. Xiao, S. I. Cho, R. Liu, S. B. Lee, *J. Am. Chem. Soc.* **2007**, *129*, 4483.
[30] L. Liang, J. Liu, J. C. F. Windisch, G. J. Exarhos, Y. Lin, *Angew. Chem. Int. Ed.* **2002**, *41*, 3665.
[31] H. D. Tran, Y. Wang, J. M. D'Arcy, R. B. Kaner, *ACS Nano* **2008**, *2*, 1841.
[32] J. Byun, J. I. Lee, S. Kwon, G. Jeon, J. K. Kim, *Adv. Mater.* **2010**, *22*, 2028.
[33] M. S. Sander, L. S. Tan, *Adv. Funct. Mater.* **2003**, *13*, 393.
[34] K. P. Musselman, G. J. Mulholland, A. P. Robinson, L. Schmidt-Mende, J. L. MacManus-Driscoll, *Adv. Mater.* **2008**, *20*, 4470.
[35] A. P. Li, F. Müller, A. Birner, K. Nielsch, U. Gösele, *J. Appl. Phys.* **1998**, *84*, 6023.
[36] S.-K. Hwang, S.-H. Jeong, H.-Y. Hwang, O.-J. Lee, K.-H. Lee, *Korean J. Chem. Eng.* **2002**, *19*, 467.
[37] S. Z. Chu, K. Wada, S. Inoue, S. Todoroki, *J. Electrochem. Soc.* **2002**, *149*, B321.
[38] S.-Z. Chu, K. Wada, S. Inoue, S.-i. Todoroki, Y. K. Takahashi, K. Hono, *Chem. Mater.* **2002**, *14*, 4595.
[39] T. F. Otero, E. de Larreta-Azelain, *J. Chim. Phys.* **1989**, *86*, 131.
[40] T. F. Otero, E. de Larreta-Azelain, R. Tejada, *Makromol. Chem., Macromol. Symp.* **1988**, *20/21*, 615.
[41] R. N. Wenzel, *Ind. Eng. Chem.* **1936**, *28*, 988.
[42] S. R. Coulson, I. S. Woodward, J. P. S. Badyal, S. A. Brewer, C. Willis, *Chem. Mater.* **2000**, *12*, 2031.
[43] M. Wolfs, T. Darmanin, F. Guittard, *Macromolecules* **2011**, *44*, 9286.
[44] L. Ionov, N. Houbenov, A. Sidorenko, M. Stamm, S. Minko, *Adv. Funct. Mater.* **2006**, *16*, 1153.
[45] L. Chen, M. Liu, H. Bai, P. Chen, F. Xia, D. Han, L. Jiang, *J. Am. Chem. Soc.* **2009**, *131*, 10467.
[46] L. D. Chambers, K. R. Stokes, F. C. Walsh, R. J. K. Wood, *Surf. Coat. Technol.* **2006**, *201*, 3642.
[47] M. Liu, X. Liu, C. Ding, Z. Wei, Y. Zhu, L. Jiang, *Soft Matter* **2011**, *7*, 4163.
[48] C. Ding, Y. Zhu, M. Liu, L. Feng, M. Wan, L. Jiang, *Soft Matter* **2012**, *8*, 9064.
[49] A. Czardybon, M. Lapkowski, *Synth. Met.* **2001**, *119*, 161.
[50] P. Schottland, O. Fichet, D. Teyssié, C. Chevrot, *Synth. Met.* **1999**, *101*, 7.
[51] T. Darmanin, M. Nicolas, F. Guittard, *Phys. Chem. Chem. Phys.* **2008**, *10*, 4322.